Thermally Forced Stationary Axisymmetric Flow on the f Plane in a Nearly Frictionless Atmosphere

VOLKMAR WIRTH

Meteorologisches Institut, Universität München, Munich, Germany

(Manuscript received 9 June 1997, in final form 6 January 1998)

ABSTRACT

This paper investigates stationary axisymmetric balanced flow of a stably stratified dry non-Boussinesq atmosphere on the f plane. The circulation is forced in the troposphere through thermal relaxation toward a specified equilibrium temperature and is damped through Rayleigh friction in the interior of the domain. Surface friction is sufficiently strong to ensure weak surface winds. As in the analogous zonally symmetric problem studied by Plumb and Hou there is threshold behavior in the frictionless limit with a thermal equilibrium solution for subcritical forcing and a highly nonlinear so-called angular momentum conserving (AMC) solution for supercritical forcing. The latter is characterized by a sharp outward edge of the vortex circulation and a nonvanishing secondary cross-vortex circulation. In the frictionless limit, the secondary circulation does not reach above the region of the thermal forcing. Noticeable differences of the current problem with respect to the zonally symmetric problem arise from the strong nonlinearity of the thermal wind equation and the nonzero thermal forcing right on the axis of symmetry. For the highly nonlinear AMC solution an approximate analytical theory is presented and verified by use of a numerical Eliassen balanced vortex model. This model is also used to investigate the nonlinear dependence of the secondary circulation on the Rayleigh friction coefficient and the penetration of the secondary circulation above the tropopause. An analytic Green's function solution for the linearized problem gives insight into nonlinear asymptotic dependences. Thinking in terms of an Eliassen balanced vortex model offers a new view on the secondary circulation in the AMC regime.

1. Introduction

The motivation for this work originated in the observation of weak but distinct minima in total ozone over monsoonal systems (Zhou and Chao 1994; Zou 1996). Viewing a monsoonal system as being forced by diabatic heating in the troposphere (Ting 1994), one may expect a secondary circulation with upward air motion in the center of the heating. To the degree that the secondary circulation extends upward into the stratosphere, it would dynamically cause a local decrease of total ozone.

We shall completely refrain from dealing with the complexities of monsoonal systems. Instead, a highly idealized problem is considered as a step toward an understanding of the underlying basic dynamics. We investigate balanced flow of a stably stratified dry non-Boussinesq atmosphere on the f plane. The flow is assumed to be rotationally symmetric about an axis perpendicular to the f plane. The circulation is forced in the troposphere through thermal relaxation toward a specified equilibrium temperature and is damped through Rayleigh friction in the interior of the domain. In addition, surface friction is sufficiently strong to ensure weak surface winds.

Plumb and Hou (1992, hereafter referred to as PH92) have shown that there exists threshold behavior in a related problem. They studied the response to subtropical thermal forcing of a zonally symmetric atmosphere on the sphere. In the inviscid limit they obtained a thermal equilibrium (TE) solution for subcritical forcing and a so-called angular momentum conserving (AMC) solution for supercritical forcing. The latter is highly nonlinear and differs from the former in that there is a nonzero secondary circulation even in the inviscid limit. For a clear distinction we refer to PH92's problem in the following as the ''zonally symmetric problem,'' while our current problem is called the ''f-plane axisymmetric problem.'' One major difference between the two idealizing geometries is that only the present one is able to represent truly local thermal forcing, which appears desirable in connection with monsoonal systems. Although the f-plane axisymmetric problem and the zonally symmetric problem share a number of features, noticeable differences arise, mostly because the thermal wind equation has a stronger nonlinearity and there is nonzero thermal forcing right on the axis of symmetry in the present case. Of course, real monsoonal systems are neither zonally symmetric nor f plane axi-

Corresponding author address: V. Wirth, Meteorologisches Institut, Theresienstraße 37, 80333 München, Germany.
E-mail: volkmar@meteo.physik.uni-muenchen.de

symmetric. Nevertheless, it is considered worthwhile to shed some light on the f-plane axisymmetric problem, too, since it represents another possible symmetry that allows a similar quasi-analytical approach to that of the zonally symmetric problem.

We will investigate the dependence of the flow on the Rayleigh friction parameter and consider, in particular, the frictionless limit. The motivation for this approach is similar to previous work (Schneider 1977; Held and Hou 1980, hereafter referred to as HH80; Lindzen and Hou 1988; Hou and Lindzen 1992; PH92): The complex circulation of the real atmosphere, being highly variable in both time and space, is idealized by constraining it to be stationary and symmetric. Comparing the frictionless limit of this idealized flow with the suitably averaged real flow then yields a particular view on the role of ''eddies,'' that is, deviations from stationarity and symmetry, which exist in real flows (cf. Schneider 1987; Becker et al. 1997). Unlike the above-quoted studies we assume a non-Boussinesq atmosphere extending far beyond the tropopause. This is similar to Dunkerton (1989), although the latter study was mainly concerned with stratospheric forcing, while we will focus on tropospheric forcing. The extension of the model domain beyond the tropopause allows us to study the penetration of the secondary circulation into the stratosphere, which may have implications for the dynamical modification of lower-stratospheric ozone or the transport of water vapor from the troposphere to the stratosphere. Similar to Dunkerton (1989), but in contrast to the other quoted studies, we will use an Eliassen balanced vortex model for the numerical calculations.

The paper is organized as follows. In section 2 we present the basic material including model equations, boundary conditions, and numerical methods of solution. Section 3 deals with threshold behavior in the frictionless limit and the subcritical regime (TE solution). Additional insight will be obtained in section 4 through an analysis of the linearized system of equations. The supercritical regime (AMC solution) is investigated in section 5. Section 6 provides a summary and discussion. Some of the more technical details are deferred to the appendixes.

2. The model

a. Model equations

We consider the primitive equations on the f plane for a dry fluid. The flow is assumed to be rotationally symmetric about the vertical axis. Moreover, it is assumed to be balanced in the sense that the equation for radial momentum can be replaced by the gradient wind equation [see (4) below]. As coordinates we use radius r and log-p altitude $z = -H \ln(p/p_0)$, where p is pressure, $H = 7000$ m is a constant scale height, and $p_0 = 1000$ hPa is a constant reference pressure. The domain considered is the whole volume above the surface. For the numerical calculations, the domain is restricted to $r \le r_{\max} = 2000$ km and $z \le z_{\max} = 35$ km, which was chosen to be considerably larger than the region of the thermal forcing (to be described below). Diabatic heating is modeled as Newtonian relaxation toward a specified temperature $T_e(r, z)$ with a constant relaxation coefficient α_n. Damping of tangential momentum is modeled as Rayleigh friction with the coefficient α_r. The equations for steady flow are

$$\left(f + \frac{\partial(ru)}{r\partial r}\right)v + \frac{\partial u}{\partial z}w = X \equiv -\alpha_r u, \tag{1}$$

$$\frac{\partial T}{\partial r}v + \left(\frac{\partial T}{\partial z} + \frac{\kappa}{H}T\right)w = Q \equiv -\alpha_n(T - T_e), \tag{2}$$

$$\frac{\partial}{\partial r}(r\rho_0 v) + \frac{\partial}{\partial z}(r\rho_0 w) = 0, \tag{3}$$

$$\frac{u^2}{r} + fu = \frac{\partial \Phi}{\partial r}, \tag{4}$$

$$\frac{\partial \Phi}{\partial z} = \frac{g}{T_s}T. \tag{5}$$

Here, u, v, and w denote the tangential, radial and vertical wind, respectively; Φ is the geopotential; T is the temperature; $\rho_0(z) = p(z)/(gH)$; f is the constant Coriolis parameter; g is the gravity acceleration; $T_s = gH/R$; R is the gas constant for dry air; $\kappa = R/c_p = 2/7$; and c_p is the specific heat at constant pressure. The symbols X and Q denote the nonconservative terms in the equation for tangential momentum and temperature, respectively. The fields u and T characterize the (primary) vortex and its circulation. Combining (4) and (5) yields the thermal wind equation

$$\left(f + \frac{2u}{r}\right)\frac{\partial u}{\partial z} = \frac{g}{T_s}\frac{\partial T}{\partial r}, \tag{6}$$

which can be used instead of (4) and (5).

Relaxation of the temperature toward a given equilibrium temperature $T_e(r, z)$ with $\partial T_e/\partial r \neq 0$ in a finite subdomain (restricted to the troposphere) will be called thermal forcing in the following (see section 2b). The term ''forcing'' does not imply a cause-and-effect relationship. The resulting diabatic heating or cooling $Q(r, z)$ is part of the solution and not given a priori. In our whole study we restrict the attention to forcing that is weak enough so that the atmosphere remains stably stratified, that is,

$$\frac{T_s}{g}N^2(r, z) \equiv S(r, z) \equiv \left(\frac{\partial T}{\partial z} + \frac{\kappa}{H}T\right) > 0, \tag{7}$$

throughout the domain. Here N is the Brunt–Väisälä frequency.

The timescale for thermal relaxation is assumed to be considerably longer than a day but considerably

shorter than a month. We choose $\alpha_n = 0.1$ day^{-1} and keep this value fixed throughout our calculations. The coefficient α_r, on the other hand, is varied within the range $0 \leq \alpha_r \leq 0.1$ day^{-1}. In our attempt to study the nearly frictionless behavior, we pushed the value of α_r in the numerical calculations as close as possible toward zero without violating a certain constraint guaranteeing the existence of the numerical solution (see below). The remaining parameters were chosen as $g = 9.81$ m s^{-2}, $R = 287$ J kg^{-1} K^{-1}, and $f = 7.292 \times 10^{-5}$ s^{-1} (corresponding to a latitude of 30°N).

For later reference we note that potential temperature is

$$\theta = Te^{\kappa z/H}, \tag{8}$$

absolute vorticity is

$$\zeta_a = f + \frac{\partial(ru)}{r\partial r}, \tag{9}$$

and the absolute angular momentum about the axis of symmetry is

$$m = \frac{f}{2}r^2 + ur = \left(\frac{f}{2} + \omega\right)r^2, \tag{10}$$

where $\omega = u/r$ denotes the angular velocity of the flow. Whenever we talk about ''angular momentum'' in the context of the f-plane axisymmetric model, we mean absolute angular momentum m as defined above.

We restrict our attention to flow for which surface drag is sufficiently strong to ensure weak surface winds, which in analytical treatment will be neglected. This excludes certain atmospheric systems like hurricanes from our consideration, but it should be an acceptable treatment for monsoonal systems. Surface drag τ_s is modeled through a linear drag law according to

$$\tau_s = -c_d u_s, \tag{11}$$

where u_s is the tangential wind at $z = 0$ and c_d is a drag coefficient. We used the value $c_d = 5 \times 10^{-3}$ m s^{-1} throughout our numerical calculations. Whenever we talk about the frictionless limit, we mean $\alpha_r \to 0$ with c_d remaining constant. The other boundaries are assumed to be stress free.

The secondary circulation (v and w) can be described in terms of a cross-vortex streamfunction $\psi(r, z)$, which is defined through

$$(r\rho_0 v, r\rho_0 w) = \left(-\frac{\partial\psi}{\partial z}, \frac{\partial\psi}{\partial r}\right), \tag{12}$$

ensuring that (3) is automatically satisfied. Considering Q and X as given, one can—by forming $gT_s^{-1}\partial(2)/\partial r - \partial[(f + 2u/r)(1)]/\partial z$—derive the following linear partial differential equation for ψ:

$$\frac{\partial}{\partial r}\left(\frac{A}{r\rho_0}\frac{\partial\psi}{\partial r} + \frac{B}{r\rho_0}\frac{\partial\psi}{\partial z}\right) + \frac{\partial}{\partial z}\left(\frac{B}{r\rho_0}\frac{\partial\psi}{\partial r} + \frac{C}{r\rho_0}\frac{\partial\psi}{\partial z}\right) = F, \tag{13}$$

with the coefficients

$$A(r, z) = \frac{g}{T_s}\left(\frac{\partial T}{\partial z} + \frac{\kappa}{H}T\right) \equiv N^2, \tag{14}$$

$$B(r, z) = -\left(f + \frac{2u}{r}\right)\frac{\partial u}{\partial z} = -\frac{g}{T_s}\frac{\partial T}{\partial r}, \tag{15}$$

$$C(r, z) = \left(f + \frac{2u}{r}\right)\left(f + \frac{\partial(ru)}{r\partial r}\right), \tag{16}$$

and the forcing term

$$F(r, z) = \frac{\partial}{\partial r}\left(\frac{g}{T_s}Q\right) - \frac{\partial}{\partial z}\left[\left(f + \frac{2u}{r}\right)X\right]. \tag{17}$$

The second equality in (15) is due to (6). An equation analogous to (13) was first derived by Eliassen (1952). Equation (13) is elliptic (and, hence, the vortex is symmetrically stable) as long as $(AC - B^2) > 0$, which had to be satisfied in all numerically determined solutions and, thus, restricted the range of values for α_r that could be used. Equation (13) allows one to diagnose the secondary circulation (ψ) from knowledge about the primary vortex circulation (u and T) and the nonconservative terms (Q and X). As boundary conditions we specify $\psi = 0$ at $r = 0$ and at $z = z_{\max}$, and $w = 0$ at $r = r_{\max}$. Since our domain is considerably larger than the size of the forcing region, our results are not sensitively dependent on the choice of the upper and outer boundary condition. At the lower boundary, the drag law (11) can approximately be translated to the following condition for ψ (cf. Schubert and Hack 1983; Wirth 1995):

$$\psi(r, 0) = \frac{r\rho_0 c_d u}{f + r^{-1}\partial(ur)/\partial r}. \tag{18}$$

The vertical position $z = 0$ is interpreted as the top of the boundary layer. Assuming that the boundary layer is infinitely shallow, the actual surface is at $z = 0_-$.

b. Basic state and thermal forcing

If the equilibrium temperature T_e is a function of altitude only, that is, $T_e = T_o(z)$, a possible solution of the problem (1)–(5) plus boundary conditions is given by $(u, v, w) = (0, 0, 0)$ and $T = T_o$. One can view $T_o(z)$ as a reference temperature profile in the absence of thermal forcing. It is specified through the corresponding potential temperature profile $\theta_o(z)$ as piecewise linear in z with $\theta_o = 300$ K at $z = 0$, $\partial\theta_o/\partial z = 4.375$ K km^{-1} for $0 \leq z \leq z_{\text{tp}}$, and $\partial\theta_o/\partial z = 38$ K km^{-1} for $z_{\text{tp}} \leq z \leq z_{\max}$. The symbol z_{tp} denotes the height of the tropopause, which is taken to be at $z_{\text{tp}} = 16$ km.

For nontrivial thermal forcing the equilibrium temperature $T_e(r, z)$ has to deviate from the reference temperature $T_o(z)$. The deviation equilibrium temperature $T'_e(r, z) = T_e(r, z) - T_o(z)$ is specified as

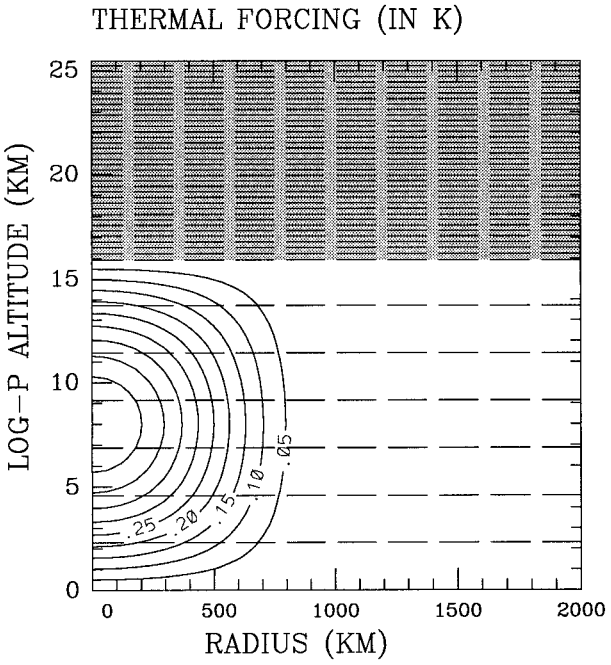

FIG. 1. Deviation equilibrium temperature $T'_e(r, z) = T_e(r, z) - T_o(z)$ (in K, solid, contours every 0.05 K, zero contour omitted) for $T_{eo} = 0.5$ K. The dashed contours indicate the reference potential temperature $\theta_o(z) = T_o(z) \exp(\kappa z/H)$ (in K, contours every 10 K) and the gray shading denotes the stratosphere.

$$T'_e(r, z) = \begin{cases} T_{eo} \sin(\pi z/z_o) \dfrac{1}{2}[1 + \cos(\pi r/r_o)] \\ \quad \text{for } r \le r_o, \qquad z \le z_o, \\ 0 \quad \text{otherwise,} \end{cases} \tag{19}$$

where $r_o = 1000$ km and $z_o = z_{\text{tp}} = 16$ km. The quantity T_{eo} is called amplitude of the thermal forcing. We restrict our attention to $T_{eo} \ge 0$, which means that we impose heating rather than cooling in the vortex center. Because of the strong nonlinearity of the model equations, some of our results do not apply to $T_{eo} < 0$.

Figure 1 shows the forcing $T'_e(r, z)$ for $T_{eo} = 0.5$ K (solid contours) and the reference potential temperature $\theta_o(z)$ (dashed contours). Note that in this and all the following altitude–radius sections only the lowermost 25 km of the computational domain are displayed. The gray shading denotes the stratosphere, which is defined via potential vorticity P as the region where $P > 4$ PVU (with 1 PVU $= 10^{-6}$ K m^2 kg^{-1} s^{-1}).

c. Numerical solution

It is possible to use (13) even in a nonstationary initial value problem, as long as the corresponding time evolution is slow (Eliassen 1952). This was exploited for solving the stationary problem (1)–(5) numerically by starting from a state at rest and integrating the time-dependent version of (1)–(5) until a steady state was reached. At each time step the cross-vortex streamfunction ψ was diagnosed by solving (13). Then the equation for tangential momentum was integrated forward by one time step using a second-order Adams–Bashforsh scheme. In addition, the temperature at the outer boundary was integrated forward in time. Finally, the temperature in the interior of the domain was calculated from the thermal wind equation (6).

One major advantage of a balanced model is that it allows a large time step. Using a grid spacing of $\Delta r = 59$ km and $\Delta z = 530$ m, we could typically take $\Delta t = 24$ h without incurring numerical instability. A more complete description of the numerical details can be found in Wirth (1995).

3. Threshold behavior in the frictionless limit

Following PH92, we call the frictionless solution with $T = T_e$ and $(v, w) = (0, 0)$ the TE solution. This solution trivially satisfies (1), (2), and (3) for any $T_e(r, z)$. Its existence hinges on whether the thermal wind equation (6) can be satisfied with $T = T_e$. Assuming that $r^{-1}\partial T/\partial r$ is finite for $r \to 0$, (6) can be rewritten as

$$\frac{\partial}{\partial z}(f\omega + \omega^2) = \frac{g}{T_s} \frac{\partial T}{r \partial r}. \tag{20}$$

With $\omega = 0$ at $z = 0$, (20) is integrated to give

$$\omega(r, z) = -\frac{f}{2} + \sqrt{\left(\frac{f}{2}\right)^2 + \Lambda(r, z)}, \tag{21}$$

where

$$\Lambda(r, z) = \frac{g}{T_s} \int_0^z \frac{\partial T(r, z')}{r \partial r}\, dz'. \tag{22}$$

In order to obtain a physical solution throughout the domain, the temperature field must be such that

$$\max\Lambda(r, z) \ge -(f/2)^2, \tag{23}$$

since otherwise ω becomes imaginary somewhere. Relation (23) yields a criterion for the existence of the TE solution through simply replacing T by T_e in the definition of Λ. With our forcing (19) one obtains

$$\omega_e = -\frac{f}{2} + \frac{f}{2}\sqrt{1 - \frac{T_{eo}}{T_c} \frac{\sin(\pi r/r_o)}{\pi r/r_o} \frac{1 - \cos(\pi z/z_o)}{2}} \qquad \text{for } r \le r_o, \quad z \le z_o, \tag{24}$$

where the subscript e denotes the TE solution and where

$$T_c = \frac{T_s}{4\pi g} \frac{r_o^2}{z_o} f^2 \tag{25}$$

plays the role of a threshold amplitude. The argument of the square root in (24) becomes negative somewhere in $[0, r_o] \times [0, z_o]$ whenever $T_{eo} > T_c$. Any forcing that

satisfies condition (23) will be called subcritical, otherwise it will be called supercritical.

The dependence of the threshold temperature on the Coriolis parameter f and the parameters defining the geometry of the forcing (r_o and z_o) in (25) is essentially the same as in the zonally symmetric problem of PH92. For the values used in this study one obtains $T_c = 0.645$ K. This can be considered as a very low threshold, and typical synoptic-scale thermal forcing in subtropical monsoonal systems is most likely supercritical. It follows that the TE solution is probably of little relevance for such real atmospheric conditions, as was already pointed out by PH92.

For supercritical forcing the TE solution does not exist. Instead, in the frictionless limit one obtains the so-called AMC solution, which will be discussed in more detail in section 5. One can also show that the AMC solution does not exist as long as the TE solution exists. Roughly speaking, in that case the term $\partial T/\partial r$ is too small for the thermal wind equation (20) to be consistent with $\omega = 0$ at the bottom and $\omega = -f/2$ at the top, which both have to be satisfied for the AMC solution. A formal proof is provided in appendix A. In short, the TE and the AMC solution are mutually exclusive. Incidentally, the ''breakdown of the gradient wind balance,'' that is, the nonexistence of the TE solution, was pointed out by Shine (1987) in the context of middle atmosphere thermal equilibrium temperatures near the summer pole.

There is marked difference concerning the threshold behavior in our case and in the zonally symmetric case of PH92. It is related to the different geometry implied by our symmetry. Both here and in PH92, the thermal wind equation is nonlinear, but the nonlinearity in PH92 is much weaker, since it involves the radius of the earth rather than the radius of the vortex in the denominator of one of its terms [cf. Eq. (5) in PH92 with our Eq. (6)]. Supercritical forcing in a zonally symmetric atmosophere means that, while the TE solution may well exist, the angular momentum about the earth's axis of rotation has a local extremum somewhere in the interior of the atmosphere. It follows that for diffusive friction the TE solution is not a regular solution of the equations; that is, it does not represent the inviscid limit of a solution with small but nonzero viscosity. On the other hand, supercritical forcing in our case means that the TE solution simply ceases to exist. In fact, as long as it exists, it is regular everywhere in the above sense (the proof is given in appendix B). In a certain sense, the strong nonlinearity of our thermal wind equation makes the problem easier.

The vortex circulation $u_e = r\omega_e$ of the TE solution (24) is plotted in Fig. 2 together with the corresponding balanced potential temperature θ_e for $T_{eo} = 0.5$ K. The balanced wind u_e reflects the forcing T'_e, since both fields are related via thermal wind balance (6). In the case of small but nonzero Rayleigh friction one expects a small deviation from the TE solution. Figure 3 illustrates the numerical solution for $\alpha_r = 2 \times 10^{-3}$ day^{-1}. Apparently, the surface friction is strong enough to keep the surface wind

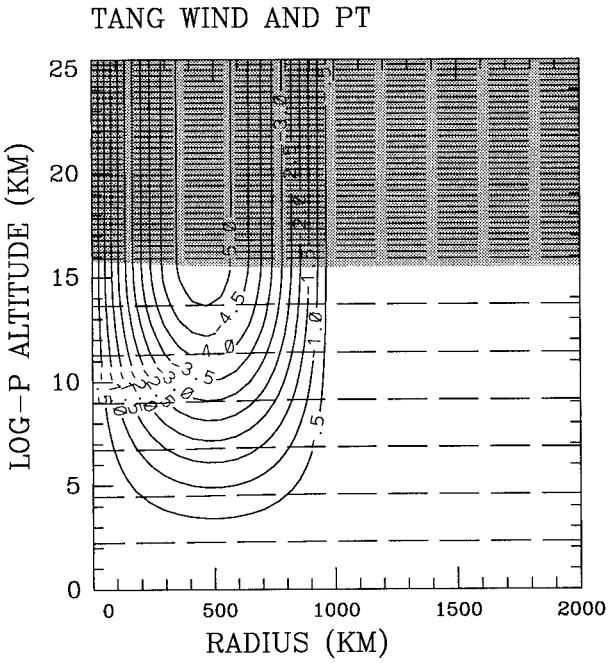

FIG. 2. The TE solution for subcritical forcing ($T_{eo} = 0.5$ K): tangential wind u_e (in m s^{-1}, solid, contours every 0.5 m s^{-1}, zero contour omitted) and potential temperature θ_e (in K, dashed, contours every 10 K). The tangential wind satisfies $u_e = 0$ at $z = 0$. The gray shading denotes the stratosphere.

close to zero. Comparison of Fig. 3a with Fig. 2 shows how close the ''nearly frictionless'' numerical solution is to the truly frictionless limit. This can be seen more systematically in Fig. 4a, where the solid line is $u_e(r, z_o)$ and the dashed lines represent numerical calculations of $u(r, z_o)$ for different values for α_r. Apparently, as the value of α_r decreases (increasing dash length), the numerical solution approaches the TE solution.

There is a nonzero cross-vortex circulation in the almost frictionless numerical solution, extending beyond the tropopause well into the stratosphere (Fig. 3b). Owing to our parameterization (18) of surface friction, the streamfunction is nonzero at the surface. The discontinuity of N^2 across the tropopause is not visible in the plot of ψ, but it would become noticeable in a plot of $v \propto \partial\psi/\partial z$ (not shown); we will come back to this point in the following section. The vertically integrated radial heat flux due to the secondary circulation is defined as

$$h(r) = \int_{0_-}^{\infty} r\rho_0 v\theta \, dz. \tag{26}$$

Numerically, this quantity is calculated as

$$h_{\text{num}}(r) = \int_0^{z_{\max}} \rho_0 r v\theta \, dz + \theta(r, 0)\psi(r, 0), \tag{27}$$

where the second term on the right-hand side accounts for the heat flux by the return flow in the boundary layer. For the TE solution, $h(r) = 0$ for all values of r,

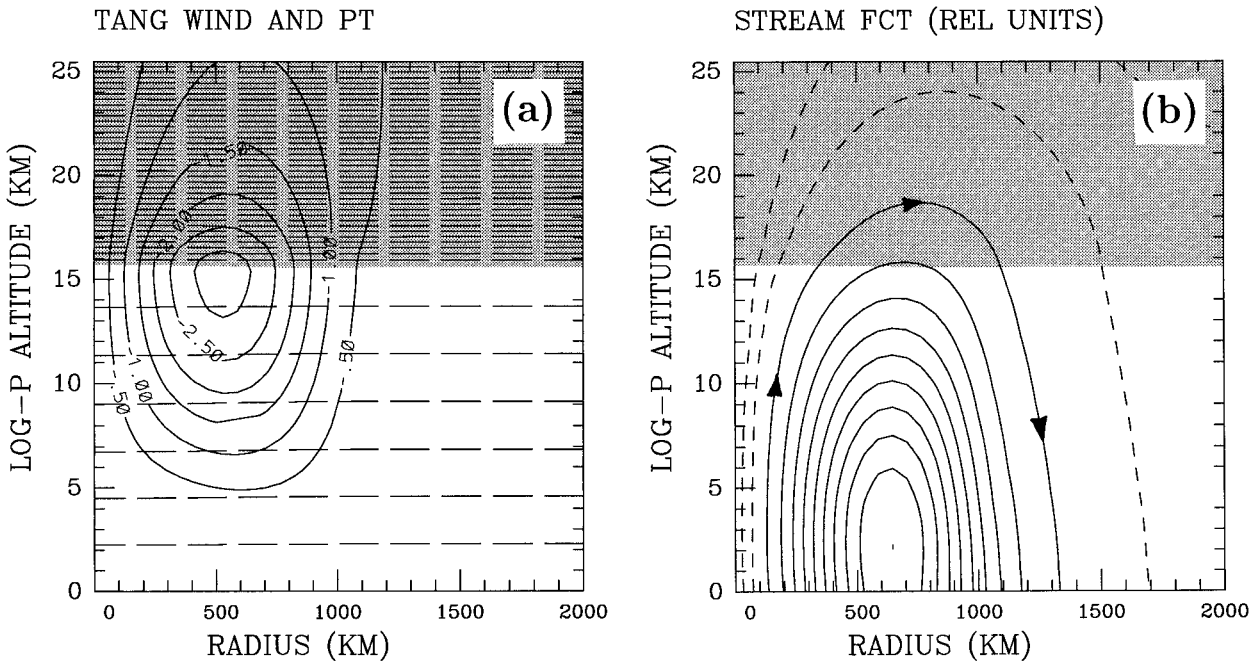

FIG. 3. Numerical solution for subcritical forcing ($T_{eo} = 0.5$ K) with small but nonzero friction $\alpha_r = 2 \times 10^{-3}$ day^{-1}. (a) Tangential wind u (in m s^{-1}, solid, contours every 0.5 m s^{-1}, zero contour omitted) and potential temperature θ (dashed contours). (b) Cross-vortex streamfunction ψ. The solid contours in (b) are drawn with a contour interval of $0.1\psi_{max}$, and the dashed contours are at $0.01\psi_{max}$ and $0.03\psi_{max}$, respectively, where $\psi_{max} = 1.95 \times 10^6$ kg s^{-1}; the arrows indicate the direction of the secondary circulation. In both panels the gray shading denotes the stratosphere.

since $\psi = 0$ everywhere. Figure 4b demonstrates, again, that the numerical solution (dashed lines) approaches the frictionless limit (solid line) as $\alpha_r \to 0$.

4. The linear regime

A key role for the nonlinear behavior of (1)–(5) is played by the absolute vorticity ζ_a. As a coefficient multiplying v in (1), ζ_a determines how strongly the radial flow interacts with the primary vortex circulation and, as a consequence, how much friction X is needed to keep the system stationary in the presence of a secondary circulation. Similarly, in the case of solid body rotation the first factor on the left-hand side of the thermal wind equation (6) is the absolute vorticity. The ratio ζ_a/f can, therefore, be taken as a measure of linearity that is relevant for both the (primary) tangential flow and its interaction with the secondary circulation. It ranges from $\zeta_a/f \approx 1$ (approximately linear) to $\zeta_a/f \approx 0$ (fully nonlinear). Figure 5 demonstrates how $\zeta_a^{\min}/f$ depends on the forcing amplitude T_{eo} and the Rayleigh friction coefficient, where $\zeta_a^{\min}$ is defined as the minimum of the absolute vorticity within the whole domain. In the frictionless limit, one obtains

$$\frac{\zeta_a^{\min}}{f} = \begin{cases} \sqrt{1 - T_{eo}/T_c} & \text{for } T_{eo} \le T_c, \\ 0 & \text{for } T_{eo} > T_c. \end{cases} \tag{28}$$

This is depicted by the solid line in Fig. 5. The three dashed lines represent numerical calculations with three different values of α_r. For $\alpha_r = 10^{-1}$ day^{-1} (short dashes), $\zeta_a^{\min} \approx f$ within the considered range of forcing amplitudes, which means that the solution is in a linear regime to a good approximation. On the other hand, for $\alpha_r = 2 \times 10^{-3}$ day^{-1} (long dashes) one obtains $\zeta_a^{\min} \approx 0$ at $T_{eo} = 5$ K, indicating that this combination of forcing and friction leads to a highly nonlinear regime. Note also that the TE solution can be highly nonlinear; that is, the two terms in the parentheses on the left-hand side of (6) can be similar in magnitude. This happens whenever T_{eo} is close to T_c. It is anticipated that linear theory gives a good approximation either when $T_{eo} \ll T_c$ (for any friction coefficient) or when the Rayleigh friction is large enough (for any forcing amplitude).

Linearizing the basic equations about the motionless reference state gives

$$fv = -\alpha_r u, \tag{29}$$

$$S_o w = -\alpha_n (T - T_e), \tag{30}$$

$$\frac{\partial}{\partial r}(r\rho_0 v) + \frac{\partial}{\partial z}(r\rho_0 w) = 0, \tag{31}$$

$$f\frac{\partial u}{\partial z} = \frac{g}{T_s}\frac{\partial T}{\partial r}, \tag{32}$$

where $S_o(z) = g^{-1}T_s N_o^2(z) = \partial T_o/\partial z + \kappa T_o/H$. Inspection of (29)–(32) shows that for any nontrivial T_e (i.e., for

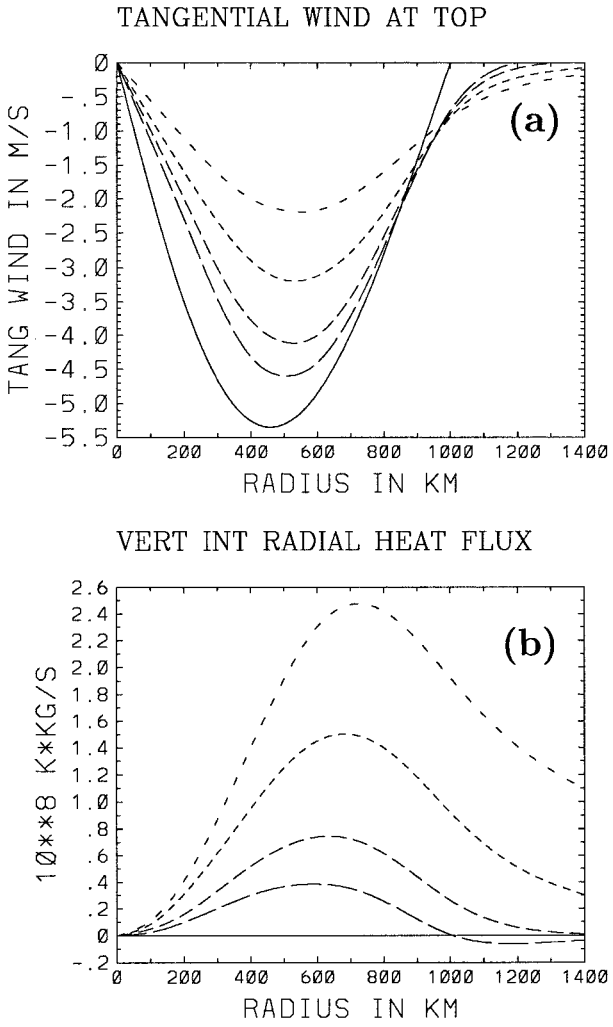

FIG. 4. Approach of the frictionless limit (TE solution) for subcritical forcing ($T_{eo} = 0.5$ K). (a) Tangential wind $u(r, z_o)$ at the top of the thermal forcing region (i.e., at z_o) as a function of radius r. (b) Vertically integrated radial heat flux $h(r)$ as a function of radius r. In both panels the solid line represents the (frictionless) TE solution. The dashed lines represent numerical calculations with $\alpha_r = 6 \times 10^{-3}$ day^{-1}, 2×10^{-3} day^{-1}, 6×10^{-4} day^{-1}, and 2×10^{-4} day^{-1}, respectively, where an increase in the length of the dashes corresponds to a decrease in α_r.

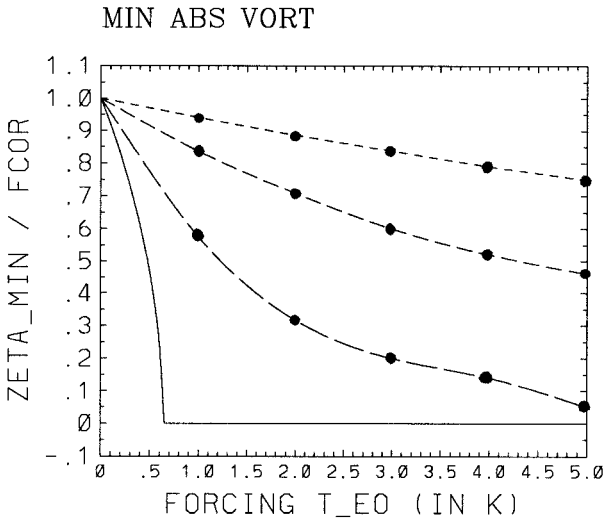

FIG. 5. Minimum absolute vorticity $\zeta_a^{\min}$ (in units of f) as function of the forcing amplitude T_{eo} (in K) for $\alpha_r = 10^{-1}$ day^{-1} (short dashes), $\alpha_r = 2 \times 10^{-2}$ day^{-1} (medium dashes), $\alpha_r = 2 \times 10^{-3}$ day^{-1} (long dashes), and in the frictionless limit (solid line). The frictionless limit represents the TE solution for $T_{eo} \leq T_c$ and the AMC solution for $T_{eo} > T_c$ ($T_c = 0.645$ K). Each dot represents a numerical solution of (1)–(5); the lines are drawn to guide the eye by connecting the respective points and have no other significance.

$\partial T_e/\partial r \neq 0$ somewhere in the domain) the TE solution exists if and only if $\alpha_r = 0$. In this sense, the secondary circulation in the linear regime can be viewed as being forced by friction, although it is by no means linear in α_r (see below).

Two measures are introduced in order to quantify two different aspects of the cross-vortex circulation with a single number each. First, the ''total strength'' is diagnosed as the maximum absolute value $\psi_{\max}$ of the streamfunction ψ. This choice is physically motivated by the fact that $2\pi\psi_{\max}$ is the total mass per unit time (in kg s^{-1}) crossing the horizontal circular area of radius $\hat{r}$ at altitude $\hat{z}$, where $(\hat{r}, \hat{z})$ is the location at which the streamfunction assumes its maximum value [this interpretation follows from the definition of ψ in (12)]. The dependence of $\psi_{\max}$ on α_r is shown in Fig. 6a. Apparently, the slope of the curve decreases with increasing α_r; in other words, the depencence on α_r is particularly sensitive as $\alpha_r \to 0$. Second, in order to quantify the stratospheric penetration of the secondary circulation, we consider the vertical wind at the vortex center at $z = 22$ km, denoted by w_{strat}. This can be taken as an approximate measure for the rate of change of total ozone due to the cross-vortex circulation. The latter is proportional to $\int w\chi_z\rho_0\, dz$, where χ_z is the vertical derivative of the ozone mixing ratio. With the tropical ozone profile from the McClatchey reference atmosphere (McClatchey et al. 1972), the function $\chi_z(z)\rho_0(z)$ has a pronounced peak at $z = 22$ km, which is why we consider the vertical wind at this particular altitude. Typical values of w_{strat} are of the order of $w_{\text{strat}} = 10^{-5}$ m s^{-1}, which for the McClatchey tropical profile corresponds to a rate of decrease of total ozone by 0.05 Dobson units per day. Figure 6b shows the dependence of w_{strat} on α_r. There is a strong increase for very small values of α_r, followed by a more gentle decrease for larger values of α_r. Thus, the stratospheric part of the secondary circulation differs qualitatively from the tropospheric part as far as its dependence on α_r is concerned.

We further investigate the dependence of the secondary circulation on α_r. For $\alpha_r \neq 0$, the linearized version of (13) is

$$r\frac{\partial}{\partial r}\left(\frac{1}{r}\frac{\partial\psi}{\partial r}\right) + \frac{\alpha_n}{\alpha_r}\frac{f^2}{N_o^2}\rho_0\frac{\partial}{\partial z}\left(\frac{1}{\rho_0}\frac{\partial\psi}{\partial z}\right) = r\rho_0\frac{\alpha_n}{S_o}\frac{\partial T_e}{\partial r} \equiv \tilde{F}(r, z). \tag{33}$$

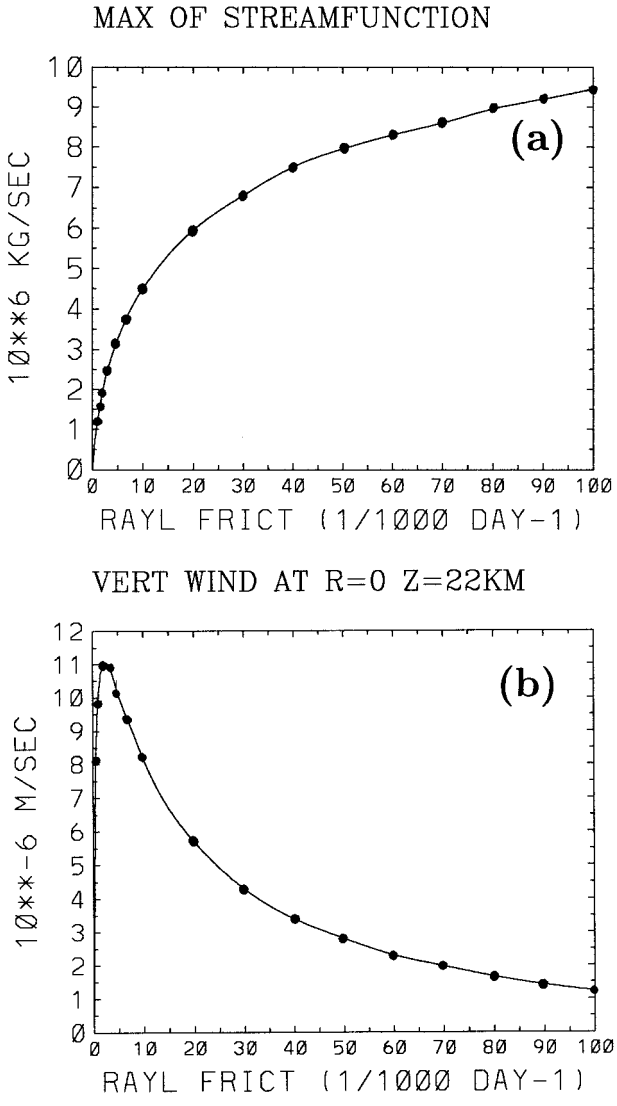

FIG. 6. Dependence of the cross-vortex circulation on the Rayleigh friction coefficient α_r for subcritical forcing (T_{eo} = 0.5 K). (a) Total strength as quantified by $\psi_{\max}$, and (b) the stratospheric part of the secondary circulation as quantified by w_{strat}. Each dot represents a numerical solution of (1)–(5). The lines connecting the dots are drawn to guide the eye and have no other significance.

Apparently, the streamfunction ψ is linear in T_e. Note that the second term of the differential operator on the left-hand side of (33) differs from the respective term in the elliptic operator connecting potential vorticity and streamfunction in standard quasigeostrophic theory. The difference is such that a discontinuity of N_o at the tropopause in the latter theory renders $\partial\psi/\partial z$ discontinuous (Bishop and Thorpe 1994), while in our case $\partial\psi/\partial z$ remains continuous. With T_{eo} from (19), the right-hand side becomes

$$\tilde{F}(r, z) = -\frac{\pi}{2}\frac{\rho_0\alpha_n}{S_o}T_{eo}\left(\frac{r}{r_o}\right)\sin(\pi r/r_o)\,\sin(\pi z/z_o) \quad \text{for } r \le r_o, \qquad z \le z_o. \tag{34}$$

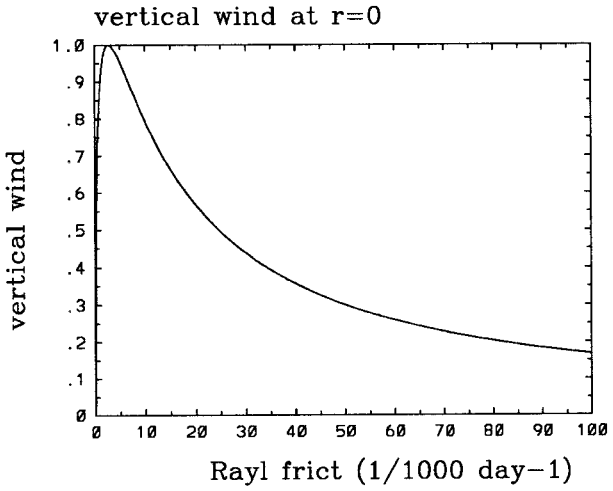

FIG. 7. Approximate analytical solution of w_{strat} according to (C10) as a function of α_r for point like forcing at $(r', z') = (r_o/2, z_o/2)$ and ρ_0 = const., N_o = const. The function is normalized so that its maximum is 1. The ratio $N_o/f = 120$ is chosen such that this calculation approximately corresponds with the numerical calculation shown in Fig. 6b.

To facilitate further progress, we discount the vertical structure of the reference state by setting ρ_0 = const. and N_o^2 = const. and replace (34) by $\tilde{F}_\delta = -r\delta(r - r')\delta(z - z')$ with $(r', z') = (r_o/2, z_o/2)$. An analytical solution to this problem is derived in appendix C. It is found that the vertical wind on the axis of symmetry, $w(0, z)$, goes asymptotically like

$$w(0, z) \sim D\sqrt{\alpha_r} \quad \text{as } \alpha_r \to 0, \tag{35}$$

where D is independent of α_r, while for large values of α_r one obtains

$$w(0, z) \ll \frac{1}{\sqrt{\alpha_r}} \quad \text{as } \alpha_r \to \infty \qquad (z \neq z'), \tag{36}$$

where $\ll$ denotes the asymptotic behavior. As a consequence $w(0, z)$ exhibits a maximum at some intermediate value of α_r. In fact, there is good qualitative agreement between the analytical solution of this simplified problem (Fig. 7) and the numerical solution shown in Fig. 6b. Similarly, it is shown in appendix C that

$$w(0, z) \sim (D/2)\sqrt{\alpha_r} \quad \text{as} \quad \alpha_r \to \infty \qquad (z = z'). \tag{37}$$

If one accepts the maximum of the vertical wind on the axis of symmetry as a measure for the strength of the secondary circulation in the troposphere, the analysis suggests that its asymptotic behavior is proportional to $\sqrt{\alpha_r}$ for both $\alpha_r \to 0$ and $\alpha_r \to \infty$. This is qualitatively consistent with the curve shown in Fig. 6a.

In order to obtain a more intuitive understanding for the dependence of w_{strat} on α_r, we note that the principal part G_1 of the Green's function G for (33) in the neighborhood of (r', z') is given by

$$G_1(r, z, r', z') = \frac{r'\rho_0 N}{2\pi f}\sqrt{\frac{\alpha_r}{\alpha_n}}\ln\sqrt{\frac{(r - r')^2}{\alpha_r} + \frac{N_o^2}{f^2}\frac{(z - z')^2}{\alpha_n}} \quad (38)$$

(cf. Eliassen 1952). The isolines of this function are ellipses centered on (r', z') with half axes in the radial and vertical direction proportional to $\sqrt{\alpha_r}$ and $\sqrt{\alpha_n} f/N_o$, respectively. Consider a point, $(r, z) \neq (r', z')$. For large α_r, the value of G_1 may be large, but the the ellipses are elongated in the radial direction and the vertical wind, which involves the radial derivative, can be rather small. For decreasing α_r, the value of G_1 decreases, but the ellipses become more and more elongated in the vertical direction such that the radial derivative and, hence, the vertical wind can increase. It is the systematic change in the aspect ratio of the ellipses that makes the streamfunction and the vertical wind behave qualitatively differently in their dependence on α_r.

5. Frictionless limit for supercritical forcing: AMC solution

Following PH92, we call the frictionless limit of the solution for supercritical forcing the angular momentum conserving (AMC) solution. As will become apparent below, the AMC solution differs qualitatively from the TE solution. It is characterized by a nonvanishing secondary circulation with upward flow in the vortex center, outward flow in the upper troposphere, downward flow at larger radii, and a return flow in the lowest part of the atmosphere. The secondary circulation modifies the temperature in such a way as to make the integration of the nonlinear thermal wind equation possible throughout the domain.

a. Thermal forcing right on the axis of symmetry

In a problem with rotational symmetry, the axis of symmetry is a singularity. In the zonally symmetric problem this singularity prevents the secondary circulation of the AMC solution from reaching the pole, since otherwise one would obtain infinite zonal wind speeds. On the other hand, the current problem involves nonzero thermal forcing right on the axis of symmetry, and the secondary circulation is nonzero right on the axis of symmetry. Fortunately this does not necessarily lead to a problem in connection with the singularity. The important difference is the sense of the secondary circulation: In the zonally symmetric cases with tropical or subtropical thermal forcing the flow toward the axis of symmetry takes place in the upper troposphere, while in the present case it takes place in the lower troposphere and, in particular, in the boundary layer. Thus, for our AMC solution to be physically meaningful it is crucial that the return flow does not conserve angular momentum. This is consistent with one of our basic assumptions, namely, nonzero boundary layer drag.

b. Numerical solution

Owing to the singularity on the axis of symmetry discussed above, it is not entirely straightforward to obtain a numerical solution for supercritical forcing and weak friction. Effectively we had to increase the depth of the boundary layer. For $\alpha_r < 2.5 \times 10^{-2}$ day^{-1}, we used

$$\hat{\alpha}_r(z) = \begin{cases} \alpha_{\rm bl} + (\alpha_r - \alpha_{\rm bl})\sin\left(\dfrac{\pi z}{2z_{\rm bl}}\right) & \text{for } z < z_{\rm bl}, \\ \alpha_r & \text{for } z \geq z_{\rm bl}, \end{cases} \quad (39)$$

instead of the constant coefficient α_r, where $\alpha_{\rm bl} = 2.5 \times 10^{-2}$ day^{-1} and $z_{\rm bl} = 5$ km, giving a smooth transition from a (moderate) value $\alpha_{\rm bl}$ at $z = 0$ to the smaller constant value α_r above $z_{\rm bl}$. Varying Rayleigh friction means varying α_r while keeping $\alpha_{\rm bl}$ constant. The use of such a modified $\hat{\alpha}_r(z)$ was necessary, since otherwise during the time integration the term $\zeta_a v$ in the time-dependent version of (1) produced strong cyclonic spin-up in the lowest few kilometers close to the axis of symmetry. Interaction of this cyclonic circulation with our parameterization of surface friction and Newtonian relaxation then precluded a steady state to be reached. It is conjectured that this problem would be less severe (or nonexistent) in the case of a zonally symmetric atmosphere in the subtropics and even less so on a zonally symmetric equatorial β plane. Only in our axisymmetric f-plane geometry does a parcel with finite absolute angular momentum at $r \neq 0$ acquire infinite cyclonic wind speed if brought toward the center of the thermal forcing in the absence of friction.

A numerical solution for supercritical forcing and small but nonzero Rayleigh friction is shown in Fig. 8. The tangential wind u (Fig. 8a) is much stronger in comparison with the previous example of subcritical forcing (Fig. 3); furthermore, it does not reflect the shape of the deviation equilibrium temperature $T'_e(r, z)$ as was the case before. Instead, the upper-tropospheric u increases approximately linearly with radius out to about $r = 950$ km. At larger radii it decays to zero rather abruptly. The tropopause is roughly 1 km above its reference position in the vortex center. There is weak cyclonic circulation in the neighborhood of $(r, z) = (500$ km, 4 km), which would be stronger if we had used α_r instead of the modified $\hat{\alpha}_r$ (see above). The modification of the Rayleigh friction coefficient is partly responsible for the qualitative differences of the cross-vortex circulation close to the lower boundary in this run (Fig. 8b) compared to the subcritical run (Fig. 3b). In addition, there seems to be a qualitative difference in the behavior of ψ at the tropopause: it appears to avoid the stratosphere and to develop a kink close to the tropopause. We will come back to this point in the following section. As a measure of absolute angular momentum about the axis of rotation, Fig. 8c shows the distribution of potential radius R; the latter is defined via $m \equiv fr^2/$

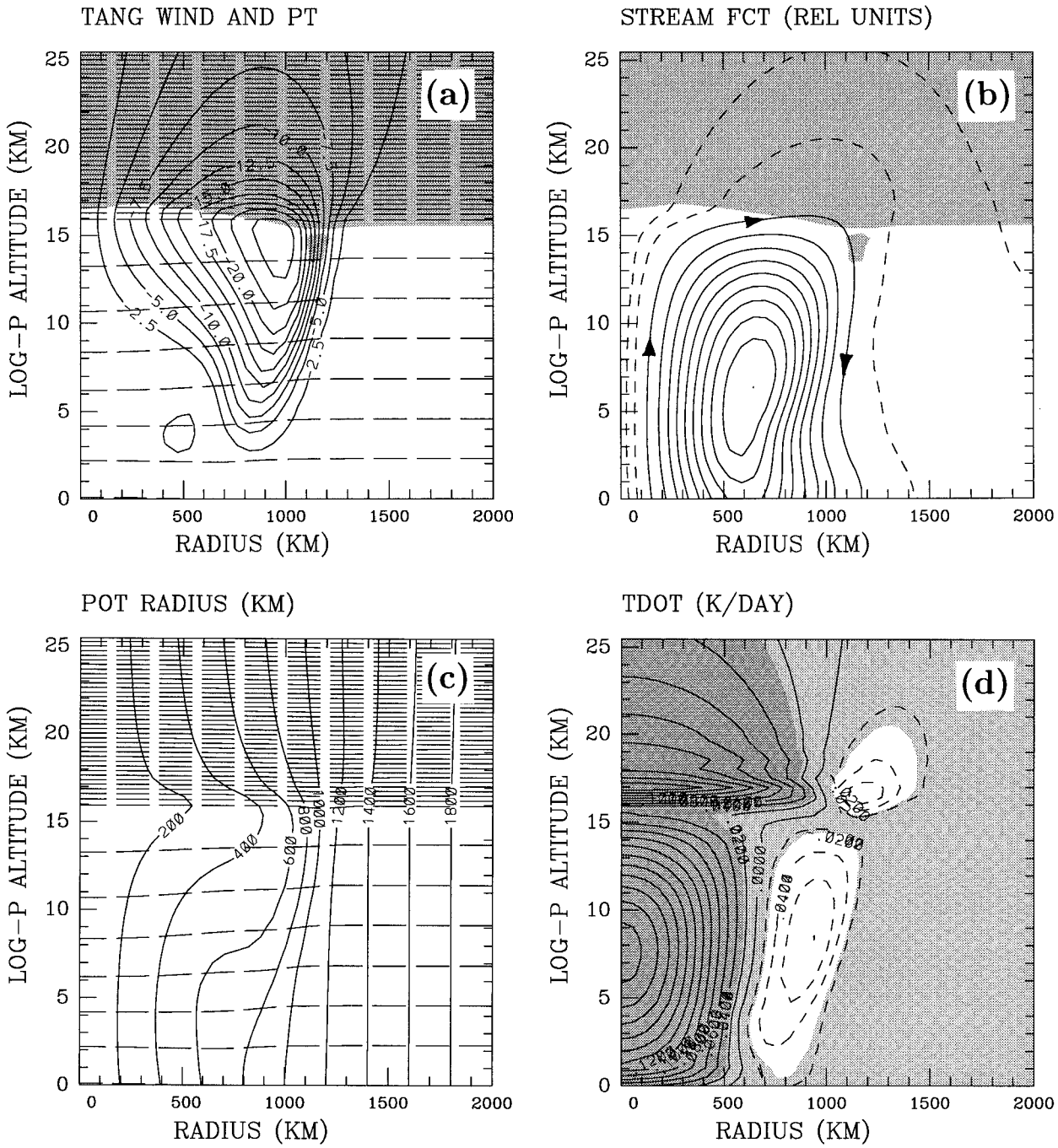

FIG. 8. Numerical solution for supercritical forcing (T_{eo} = 5 K) with small but nonzero friction $\alpha_r = 2 \times 10^{-3}$ day^{-1}. (a) Tangential wind u (in m s^{-1}, solid, contours every 2.5 m s^{-1}, zero contour omitted) and potential temperature θ (dashed contours). (b) Cross-vortex streamfunction ψ, with plotting conventions as in Fig. 3b; the maximum value of the streamfunction is $\psi_{max} = 3.8 \times 10^7$ kg s^{-1}. (c) Potential radius R (in km, solid contours) and potential temperature θ (dashed contours). (d) Diabatic heating Q (in K day^{-1}, contours every 0.02 K day^{-1}, solid contours and dark shading for positive values, dashed contours and white shading for negative values).

$2 + ur = fR^2/2$, so that lines of constant R are lines of constant m. Apparently, the circulation is approximately angular momentum conserving: the contours of R are approximately parallel to the contours of ψ except where friction is large, that is, except close to the lower boundary (where $\hat{\alpha}_r \neq 0$) and in the upper troposphere (where u is large and, hence, X is nonnegligible). Figure 8d gives the diabatic heating Q, illustrating that there is heating in regions of upward motion and cooling in regions of downward motion; in addition, the

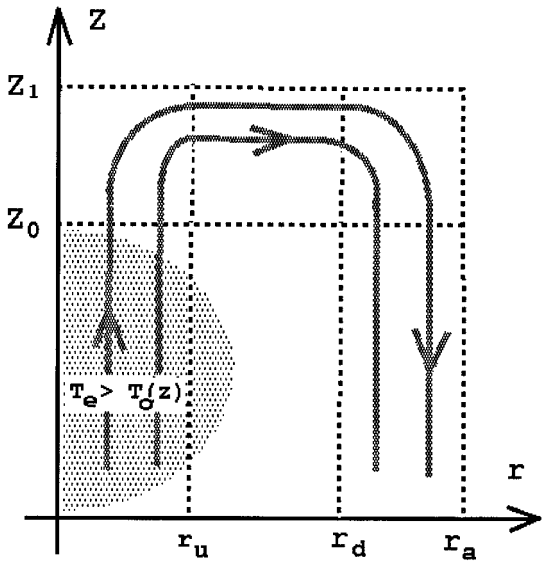

FIG. 9. Schematic illustration of a hypothetical situation in which the AMC solution extends to an altitude, z_1, that is above the top z_o of the thermal forcing region. The thermal forcing region is marked by gray shading. In the radial direction the secondary circulation extends out to radius r_a. Furthermore, r_u and r_d are defined such that there is upwelling for $0 \le r \le r_u$ and downwelling for $r_d \le r \le r_a$.

change in static stability at the tropopause is clearly visible.

c. Vertical extent of the secondary circulation

The secondary circulation of the AMC solution cannot extend beyond the maximum altitude z_o of the thermal forcing. We are going to prove this statement by assuming the opposite and deriving a contradiction to this assumption. Figure 9 serves for illustration.

Assume that the secondary circulation extends up to altitude $z_1 > z_o$, but that the thermal forcing does not reach beyond z_o, that is, $T_e' = 0$ for $z > z_o$. Further, let r_a be the maximum radius out to which the secondary circulation extends. Owing to angular momentum conservation, a parcel in stationary flow moving radially outward at altitude $z = z_1$ starting at $r = 0$ has

$$\omega(r, z_1) = -f/2 \quad \text{for} \quad 0 \le r \le r_a; \tag{40}$$

see (10). Integration of the thermal wind equation (20) from z_o to z_1 together with (40) gives

$$\omega(r, z_o) = -\frac{f}{2} + \sqrt{-\frac{g}{rT_s}\int_{z_o}^{z_1} \frac{\partial T(r, z)}{\partial r}\, dz}$$

$$= -\frac{f}{2} + \sqrt{-\frac{g(z_1 - z_o)}{rT_s}\frac{\partial \tilde{T}}{\partial r}}, \tag{41}$$

where the tilde denotes a vertical average between z_o and z_1. Consider two radii r_u and r_d such that between z_o and z_1 there is upwelling for $0 \le r \le r_u$ and downwelling for $r_d \le r \le r_a$. Since in our whole study we assume a statically stable atmosphere, this renders $\tilde{T} < \tilde{T}_e$ for $0 \le r \le r_u$ and $\tilde{T} > \tilde{T}_e$ for $r_d \le r \le r_a$. By assumption we have $T_e' = 0$ and, therefore, $T_e = T_o(z)$ for $z \ge z_o$. It follows that $\tilde{T}_e = $ const. and, hence, $\partial\tilde{T}/\partial r > 0$ somewhere in $0 \le r \le r_a$, resulting in a negative argument of the square root in (41). The initial assumption thus leads to an unphysical solution in connection with the nonlinear thermal wind equation. It follows that the secondary circulation cannot extend to altitudes higher than z_o.

We come back to the kink in the streamfunction close to the tropopause mentioned in connection with Fig. 8b. This near discontinuity of $\partial\psi/\partial z$ arises because Eq. (13) ceases to be elliptic in the limit $\alpha_r \to 0$. Of course, in the numerical calculation the condition $AC - B^2 > 0$ is satisfied everywhere, but in the neighborhood of the tropopause for $0 \le r \le r_a$ the coefficient C is only a small fraction compared with its value in the linear case. This means that the penalty of high curvature $\partial^2\psi/\partial z^2$ becomes low, allowing the solution to develop high values of $\partial^2\psi/\partial z^2$ at $z = z_o$. In this sense, the kink is a property of the elliptic equation (13) in the limit $\alpha_r \to 0$. On the other hand, a kink in ψ across the tropopause is equivalent to a discontinuity of the velocity component parallel to the tropopause, allowing nonzero tropopause-parallel flow in the troposphere right underneath the tropopause but, at the same time, zero flow right above the tropopause. Thus, the kink of ψ in the almost frictionless numerical solution reflects the fact that in the limit $\alpha_r \to 0$ the cross-vortex circulation cannot penetrate above z_o.

d. Approximate analytical theory

We shall now present an approximate analytical theory for the AMC solution and compare it with with corresponding numerical integrations. It was shown in the previous section that $\psi_a = 0$ for $z > z_o$, where the subscript a denotes the AMC solution. As a consequence, $T = T_e = T_o(z)$ and $\partial u/\partial z = 0$ for $z > z_o$. One can restrict attention to $z \le z_o$ and proceed in a similar way as HH80 or PH92. Consider a parcel in the vortex center that is lifted up to altitude z_o and subsequently advected radially outward to some radius r_a. Since $m = 0$ in the vortex center, it follows from (10) and the conservation of angular momentum that along the parcel's streamline

$$\omega_a(r, z_o) = -f/2 \quad \text{in} \quad 0 \le r \le r_a \tag{42}$$

or, equivalently,

$$u_a(r, z_o) = -(f/2)r \quad \text{in} \quad 0 \le r \le r_a. \tag{43}$$

For $r > r_a$ the secondary circulation is assumed to be zero and the tangential wind to be in thermal wind balance with T_e. Note that (43) renders the factor multiplying v in (1) equal to zero for $0 \le r \le r_a$ at $z = z_o$. In contrast to the situation with the linearized equation (29), the nonlinearity allows nonzero v even for $\alpha_r = 0$.

Consider the vertical average over the depth of nonzero secondary circulation, denoted by an overbar like

$$\overline{T}(r) = \frac{1}{z_o}\int_{0_-}^{z_o} T(r, z)\, dz. \tag{44}$$

Here, $z = 0_-$ denotes the earth's surface, as opposed to $z = 0$, which is the top of the boundary layer at which ψ is not necessarily zero [owing to (18)]. The vertical average of (20) gives

$$\omega^2(r, z_o) + f\omega(r, z_o) = \frac{gz_o}{T_s r}\frac{\partial \overline{T}}{\partial r}, \tag{45}$$

where it has been used that $\omega = 0$ at the earth's surface. Multipliying by r, using (42), and integrating radially leads to

$$\overline{T}_a(r) = T_{ao} - \frac{\pi}{2}T_c\left(\frac{r}{r_o}\right)^2 \quad \text{for } 0 \le r \le r_a. \tag{46}$$

The constants T_{ao} and r_a are obtained by invoking the conservation of energy and the continuity of the temperature field. The heat equation (2) together with (3) is rewritten in terms of potential temperature as

$$\frac{\partial}{\partial r}(r\rho_0 v\theta) + \frac{\partial}{\partial z}(r\rho_0 w\theta) = -\alpha_n r\rho_0(\theta - \theta_e). \tag{47}$$

Integration of (47) over the whole region of nonzero secondary circulation gives

$$0 = \int_0^{r_a} \alpha_n r\overline{\rho_0(\theta_a - \theta_e)}\, dr. \tag{48}$$

We do the following approximations:

$$\overline{\rho_0\theta} \approx \overline{\rho}_0\overline{\theta} \approx \overline{\rho}_0\overline{e^{\kappa z/H}}\,\overline{T}, \tag{49}$$

where in the case of the reference temperature profile the first and the second approximation overestimates the true value by 3.8% and 2.5%, respectively. Recalling that α_n = const., (48) with (49) becomes

$$0 = \int_0^{r_a} (\overline{T}_a - \overline{T}_e) r\, dr. \tag{50}$$

Equation (50), which is our f-plane axisymmetric analogue of the ''equal-area'' construction in HH80, fixes T_{ao} and r_a in (46). Some more details are given in appendix D.

The dependence of the radius r_a on the forcing amplitude T_{eo} is shown in Fig. 10. For marginally supercritical forcing the dependence is very sensitive. As shown in appendix D, $r_a = r_o$ for $T_{eo}/T_c = (\pi/2)^2(1 - 4/\pi^2)^{-1} \approx 4.15$, that is, for $T_{eo} = 2.68$ K. At higher forcing amplitudes, the dependence becomes rather weak, with r_a increasing from 1200 to 1400 km between $T_{eo} = 5$ and 10 K.

We tested the prediction (43) of the approximate analytical theory for $u(r, z_o)$ by running the numerical model with $T_{eo} = 5$ K and different values of α_r. Figure 11a shows the result. As the value of α_r decreases, the numerical solution (dashed lines, with increasing dash length for decreasing α_r) broadly approaches the theoretical prediction (solid line); in particular, the predicted radius r_a appears to be relevant for the numerical solution for small values of α_r. For small radii, the slope $\partial u/\partial r$ of the numerical solutions is somewhat smaller than predicted. This is similar to a feature found by HH80 and is believed to be (partly) due to the width of the rising branch of the secondary circulation.

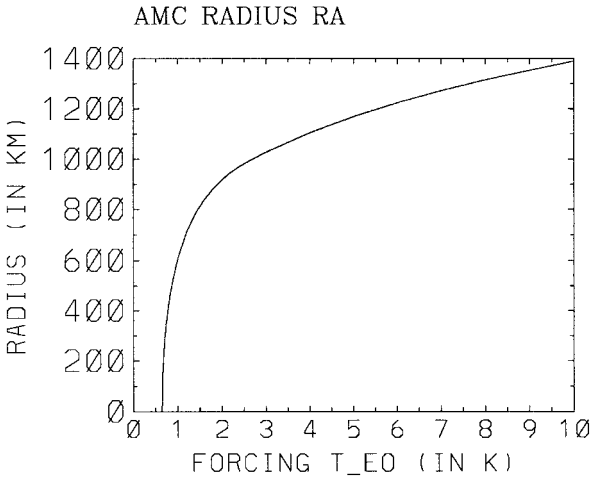

FIG. 10. Dependence of the radius r_a on the forcing amplitude T_{eo}. The parameter r_a is the maximum radius out to which the secondary circulation extends in the AMC regime according to the approximate analytical theory.

e. Secondary circulation

The vertical integral of (47) from 0_- to ∞ gives

$$\frac{dh}{dr} = -\alpha_n r z_o\overline{\rho_0(\theta_a - \theta_e)} \approx -\alpha_n z_o r\overline{\rho}_0\overline{e^{\kappa z/H}}(\overline{T}_a - \overline{T}_e). \tag{51}$$

Since both $\overline{T}_e(r)$ and $\overline{T}_a(r)$ are known, this equation can readily be integrated with $h = 0$ at $r = 0$ to yield $h(r)$. The result is displayed as a solid curve in Fig. 11b. Comparison with the numerical solution (dashed lines) suggests, again, a fairly good agreement in the limit $\alpha_r \to 0$.

Figure 12 shows the dependence of $\psi_{\max}$ and w_{strat} on α_r for $T_{eo} = 5$ K. For the larger values of α_r displayed in the figure, both the total strengh and the stratospheric portion of the secondary circulation are a factor of 10 times larger than in Fig. 6, where we had $T_{eo} = 0.5$ K. This is consistent with the analysis of linearity from Fig. 5 and the result that $\psi \propto T_{eo}$ in the linear regime [see (33)]. Significant nonlinearity appears in Fig. 12 at small values of α_r, for which the actual curve (solid line) deviates from the curve that one would obtain from the linearized equations (dashed curve). Linear theory underpredicts $\psi_{\max}$ while it overpredicts w_{strat}. The qual-

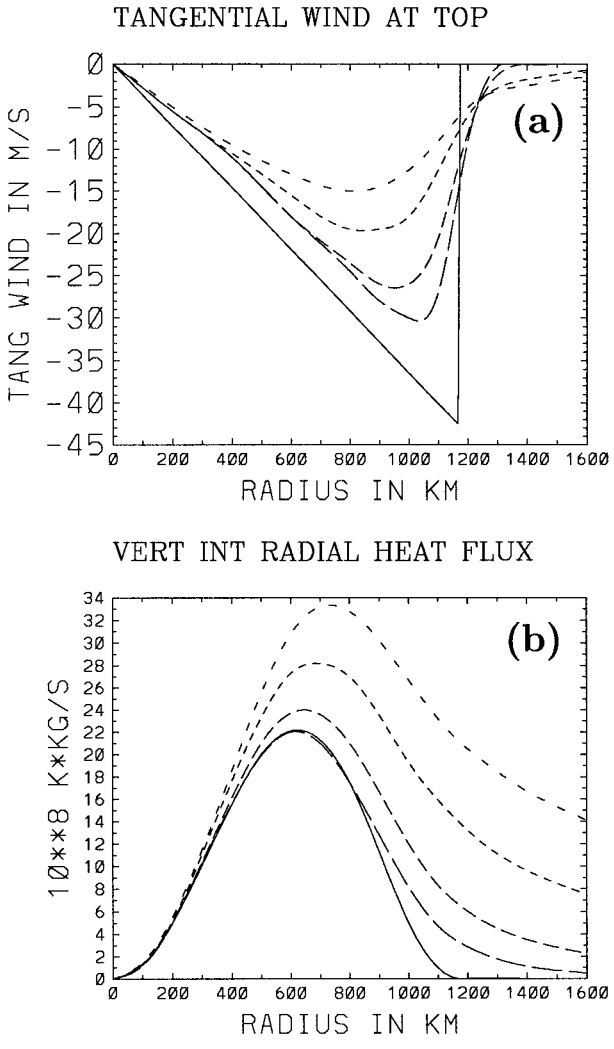

FIG. 11. Approach of the frictionless limit (AMC solution) for supercritical forcing (T_{eo} = 5 K). (a) Tangential wind $u(r, z_o)$ at the top of the thermal forcing region (i.e., at z_o) as a function of radius r. (b) Vertically integrated radial heat flux $h(r)$ as a function of radius r. In both panels the solid line represents the (frictionless) AMC solution according to the approximate analytical theory. The dashed lines represent numerical calculations with $\alpha_r = 10^{-2}$ day^{-1}, 5×10^{-3} day^{-1}, 2×10^{-3} day^{-1}, and 10^{-3} day^{-1}, respectively, where an increase in the length of the dashes corresponds to a decrease in α_r.

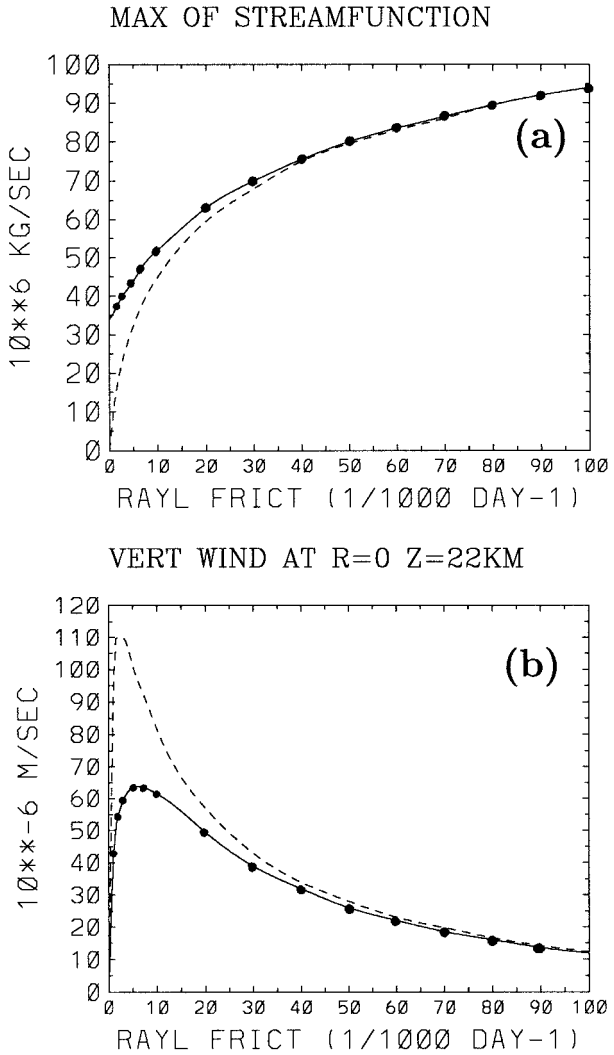

FIG. 12. Dependence of the cross-vortex circulation on the Rayleigh friction coefficient α_r for supercritical forcing (T_{eo} = 5 K). (a) Total strength as quantified by ψ_{max} and (b) the stratospheric part of the secondary circulation as quantified by w_{strat}. Each dot represents a numerical solution of (1)–(5). The solid lines connecting the dots are drawn to guide the eye and have no other significance. The dashed lines represent the respective solid lines from Fig. 6 after multiplication by 10; that is, they indicate the hypothetical functional dependence on α_r if the dependence on T_{eo} were linear.

itative dependence of w_{strat} on α_r is similar in the subcritical and the supercritical regime, with $w_{strat} \to 0$ for both $\alpha_r \to 0$ and $\alpha_r \to \infty$. On the other hand, there is clearly a qualitative difference between subcritical and supercritical forcing for ψ_{max} as $\alpha_r \to 0$: while $\psi_{max} \to 0$ for subcritical forcing, $\psi_{max} \to$ const. $\neq 0$ for supercritical forcing. This reflects the distinguishing property of the AMC solution to have a nonzero secondary circulation.

6. Summary and discussion

We investigated stationary axisymmetric balanced flow of a stably stratified dry non-Boussinesq atmosphere on the f plane. The circulation is forced in the troposphere through thermal relaxation toward a specified equilibrium temperature and is damped through Rayleigh friction in the interior of the domain. Surface friction is sufficiently strong to ensure weak surface winds. In contrast to the zonally symmetric problem of PH92, the geometry of the current problem is able to represent truly local thermal forcing. We studied the dependence of the flow on the strength of friction with particular focus on the frictionless limit, and we investigated the upward penetration of the secondary circulation into the stratosphere. Both approximate analytical and numerical calculations were performed; for the lat-

ter an Eliassen balanced vortex model was used. Our main results are the following.

1) There is threshold behavior in the frictionless limit with a thermal equilibrium (TE) solution for subcritical forcing and a so-called angular momentum conserving (AMC) solution for supercritical forcing. The existence of a threshold separating two qualitatively different regimes is quite analogous to the corresponding result of PH92 for the zonally symmetric case.
2) By definition, the TE solution has a primary vortex circulation that reflects the equilibrium temperature, while its secondary (cross vortex) circulation is zero. When the forcing is subcritical, but close to the critical threshold, the TE solution is strongly nonlinear in the sense that the nonlinear term in the thermal wind equation is about as important as the linear term. In contrast to the zonally symmetric problem, the TE solution does not exist for supercritical forcing and it is regular throughout its range of existence (i.e., for subcritical forcing). The difference arises from the stronger nonlinearity of the thermal wind equation in the current problem compared with the zonally symmetric problem. Here, a solution is called regular if it can be the inviscid limit of a solution with nonzero viscosity.
3) The AMC solution is characterized by a sharp outward edge of the primary vortex circulation and a nonvanishing secondary circulation with upward flow in the vortex center. In contrast to the zonally symmetric problem, the singularity at the axis of symmetry poses no constraint on the the secondary circulation, since its sense is such that the flow toward the axis of symmetry takes place in the boundary layer, which is not frictionless by assumption. For forcing that is well into the supercritical regime, the location of the outward edge depends only weakly on the amount of the forcing. Similar to the zonally symmetric problem one can find an approximate analytical theory for the AMC solution; it predicts well the salient features of the numerical solution for small (but nonzero) friction.
4) For small but nonzero friction our numerical Eliassen balanced vortex model approximately represents the (strictly speaking hypothetical) AMC solution. This success suggests that one can view the nonzero secondary circulation in the AMC regime as a thermally and frictionally forced Eliassen cross-circulation in the limit of small friction.
5) The cross-vortex circulation of the AMC solution cannot extend above the maximum altitude of the thermal forcing. For thermal forcing that is confined to the troposphere it means that the cross-vortex circulation cannot extend into the stratosphere. This property of the AMC solution is consistent with the behavior of the elliptic equation for the Eliassen secondary circulation when friction becomes small.
6) The overall strength of the secondary circulation in the troposphere increases monotonically, albeit nonlinearly with the friction coefficient. On the other hand, the impact of the secondary circulation on the stratosphere (as quantified by the vertical wind in the vortex center) has a maximum at an intermediate value of the friction coefficient and decreases for larger values. These dependencies are a property of the elliptic equation for the Eliassen secondary circulation in the linearized problem and are reproduced by the asymptotic behavior of the corresponding Green's function solution.

It is not exactly straightforward to put these results into the context of the original motivation, namely, the dynamics of monsoonal systems. Although a monsoonal system may persist for several months, it is by definition a transient phenomenon, and one may ask to what degree a stationary flow regime is relevant at all. Our numerical method of solution gives us a clue, since it involves a switch-on time integration that, in a certain sense, simulates the onset of a monsoon. In the experiment shown in Fig. 8, both the primary and the secondary circulation in the troposphere had practically reached their steady-state limit after about 150 days, with their general characteristics being established even earlier. In view of the rather long timescale τ_n we used for the thermal forcing ($\tau_n = \alpha_n^{-1} = 10$ days), it may not be completely unreasonable to assume that a monsoonal system persists long enough that stationary flow has some relevance for the tropospheric part of the circulation.

In the stratosphere, on the other hand, it takes considerably longer for the circulation to reach a steady state (5–10 times longer in the quoted experiment at 10 km above the tropopause compared with the troposphere). As a consequence, our result that the stationary secondary circulation cannot extend into the stratosphere in the frictionless limit is not relevant on the timescale of one season. In the time-dependent problem, the secondary circulation extends well into the stratosphere during a considerable amount of time even in the complete absence of friction. It will decay to zero only as the steady state is approached. Immediately after switch on with an initial atmosphere at rest, (13) becomes

$$r\frac{\partial}{\partial r}\left(\frac{1}{r}\frac{\partial \psi}{\partial r}\right) + \frac{f^2}{N_o^2}\rho_0\frac{\partial}{\partial z}\left(\frac{1}{\rho_0}\frac{\partial \psi}{\partial z}\right) = \tilde{F}(r, z). \quad (52)$$

This equation is almost identical to (33), which is relevant for the stationary limit, *except* for the factor α_n/α_r missing in front of the second term on the left-hand side. Since (52) is a truly elliptic equation independent of the values of α_r and α_n, its solution ψ extends beyond the forcing region. This (transient) secondary circulation will dynamically affect ozone and may transport water vapor from the troposphere into the stratosphere. For moderate and higher values of the friction coefficient ($\alpha_r \geq 10^{-2}$ day^{-1}), both the tropospheric and the strat-

ospheric circulation reached a steady state within about 150 days. A full discussion of the various timescales involved is beyond the scope of this paper.

Our parameterization for friction was deliberatly chosen to be the simplest possible, since it facilitated an approximate analytical investigation of the dependence on friction in the linearized regime. As far as the frictionless limit is concerned, the exact parameterization of friction shoud be irrelevant. In fact, we did some numerical experiments with a viscous parameterization instead of Rayleigh friction and found broadly similar results.

Many of our results depend on the assumed relaxational character of the thermal forcing. Such an approach is often accepted for global studies, since the differential solar radiation externally forces horizontal temperature differences toward which the actual atmosphere relaxes through a combination of dynamics and various diabatic processes. In a monsoonal system, on the other hand, the diabatic heating is dominated by moist convection, and a simple parameterization in terms of Newtonian relaxation is more questionable. It is true that moist convection is sometimes parameterized as relaxation toward an equilibrium atmosphere, which in turn is determined by surface and boundary layer conditions (e.g., Raymond 1994). Nevertheless, the relaxation toward a specified equilibrium profile can be accepted as a first approximation only to the degree that these surface conditions are not affected by the flow itself. The latter may be a poor assumption in the context of a monsoonal system and the differences between a dry and a moist model may be significant (e.g., Hunt 1973).

The symmetry exploited in the present work crucially depends on the f-plane approximation. Breaking this symmetry, for example, by going over to the β-plane approximation, is likely to result in important changes in the character of the solution. There is work in progress that investigates the consequences of breaking the symmetry (Hsu and Plumb 1997).

In conclusion, the dynamics of real monsoonal systems certainly depend on flow asymmetries, on transient effects, on the more complicated interactions between dynamics and diabatic effects, and on the precise way of momentum damping. Nevertheless, the basic features of the idealized flow investigated in this paper and the differences with respect to the related zonally symmetric problem may prove a helpful step toward an understanding of the complex interactions in fully three-dimensional time-dependent models with realistic physical parameterizations and, eventually, in the real atmosphere.

Acknowledgments. The author wants to thank his colleagues, especially M. Juckes, for numerous stimulating discussions. The instructive comments of three anonymous reviewers are gratefully acknowledged.

APPENDIX A

Nonexistence of the AMC Solution for Subcritical Forcing

We want to prove that the AMC solution does not exist for subcritical forcing. This is done by assuming that both the TE and the AMC solution exist and showing that this assumption leads to a contradiction. The argument is similar to that in PH92.

The square of the absolute angular momentum, defined in (10), is

$$m^2 = \left(\frac{f}{2}r^2\right)^2 + \omega^2 r^4 + f\omega r^4. \tag{A1}$$

Multiplication of the vertical average thermal wind equation (45) by r^4, together with (A1), yields

$$m^2(r, z_o) = \left(\frac{f}{2}r^2\right)^2 + r^3\frac{gz_o}{T_s}\frac{\partial \overline{T}}{\partial r}. \tag{A2}$$

This equation is applied to the TE and the AMC solutions, which are both assumed to exist. The resulting two equations are subtracted from each other, yielding

$$r^3\frac{gz_o}{T_s}\left(\frac{\partial \overline{T}_a}{\partial r} - \frac{\partial \overline{T}_e}{\partial r}\right) = m_a^2(z_o) - m_e^2(z_o) = -m_e^2(z_o) \le 0$$

$$\text{for all } r \in [0, r_a]. \tag{A3}$$

Here we used that by construction $m_a^2(z_o) = 0$ in $0 \le r \le r_a$ for the AMC solution. Furthermore, the assumed existence of the TE solution guarantees that $\omega_e + f/2$ is real and nonnegative everywhere [see (21)]. It follows that $m_e(r, z_o) \ge 0$ [see (10)], which explains the $\le$ in (A3).

For energetic reasons—in order for a stationary state to be maintained against surface friction—the cross-vortex circulation of the AMC solution must be upward in a relatively warm region and downward in a relatively cold region. Therefore, and because the equilibrium temperature is higher in the vortex center than its environment, the secondary circulation must be upward in the vortex center and downward in the environment. This secondary circulation keeps the actual vertical mean temperature $\overline{T}_a$ below the equilibrium temperature $\overline{T}_e$ in the vortex center and above $\overline{T}_e$ in the environment, but at the same time it is weak enough so that the actual temperature $\overline{T}_a$ is still warmer in the vortex center than in the environement. It follows that

$$\frac{\partial \overline{T}_a}{\partial r} - \frac{\partial \overline{T}_e}{\partial r} > 0 \quad \text{at some } r_i \in [0, r_a], \tag{A4}$$

which is incompatible with (A3). From this contradiction we conclude that the AMC solution cannot coexist with the TE solution for subcritical forcing.

APPENDIX B

Regularity of the TE Solution

We define regularity as previous authors have done. When friction is modeled as vertical viscosity (with coefficient ν), (1) can be rewritten in terms of absolute angular momentum as

$$v\frac{\partial m}{\partial r} + w\frac{\partial m}{\partial z} = \frac{1}{\rho_0}\frac{\partial}{\partial z}\left(\nu\rho_0\frac{\partial m}{\partial z}\right). \tag{B1}$$

With the help of the continuity equation (3), this becomes

$$\frac{\partial}{\partial r}(r\rho_0 vm) + \frac{\partial}{\partial z}(r\rho_0 wm) = \frac{\partial}{\partial z}\left(\nu r\rho_0\frac{\partial m}{\partial z}\right). \tag{B2}$$

This equation prohibits the existence of closed contours of m in the interior for any solution with small but nonzero viscosity; the argument has been given several times before (e.g., HH80; PH92). In our case, the axis of symmetry deserves special attention, because in a certain sense it is ''in the interior'' of the flow and there is a global minimum of the angular momentum ($m = 0$ at $r = 0$ and $\partial m/\partial r > 0$ for $r > 0$; see below). Yet this poses no problem in terms of regularity, since the effect of vertical diffusion is zero at $r = 0$ (because $\partial m/\partial z = 0$ at $r = 0$). Correspondingly, the condition for regularity of a frictionless solution in our f-plane axisymmetric case is is that there can be no extrema of absolute angular momentum away from the axis of symmetry except on the lower boundary.

The angular velocity ω_e of the TE solution satisfies

$$\omega_e > -f/2 \tag{B3}$$

everywhere, which follows from (21) and where we excluded the marginally critical case. Forming $r^{-1}\partial[r^2(\text{B3})]/\partial r$ leads to

$$\zeta_{ae} \equiv f + \frac{\partial(ru_e)}{r\partial r} > 0, \tag{B4}$$

with $u_e = r\omega_e$, which proves that

$$\frac{\partial m_e}{\partial r} = r\zeta_{ae} > 0 \quad \text{for } r > 0. \tag{B5}$$

It follows that there can be no local extremum of absolute angular momentum for the TE solution away from the axis of symmetry and that, therefore, the existence of the TE solution includes its regularity.

APPENDIX C

Green's Function for the Linear Problem

Consider (33) with the right-hand side replaced by $\tilde{F}_\delta(r, z) = -r\delta(r - r')\delta(z - z')$, where $(r', z') = (r_o/2, z_o/2)$. Assuming that $\rho_0 = \text{const.}$ and $N_o = \text{const.}$ and rescaling the vertical coordinate according to $z \to N_o z/f$ leads to the following problem:

$$r\frac{\partial}{\partial r}\left(\frac{1}{r}\frac{\partial\psi}{\partial r}\right) + \frac{\alpha_n}{\alpha_r}\frac{\partial^2\psi}{\partial z^2} = -r\delta(r - r')\delta(z - z'). \tag{C1}$$

The boundary conditions are $\psi \to 0$ as $z, r \to \infty$, $0 < w = (r\rho_0)^{-1}\partial\psi/\partial r < \infty$ at $r = 0$, and $\partial\psi/\partial z = 0$ at $z = 0$. The last condition is motivated by our numerical results (Fig. 3). In this appendix we will derive a solution to (C1) plus boundary conditions and investigate its asymptotic dependence on α_r.

Introducing $\Phi = \psi/r$ gives

$$r^2\frac{\partial^2\Phi}{\partial r^2} + r\frac{\partial\Phi}{\partial r} - \Phi + r^2\frac{\alpha_n}{\alpha_r}\frac{\partial^2\Phi}{\partial z^2} = -r^2\delta(r - r')\delta(z - z'). \tag{C2}$$

With

$$\Phi(r, r', z - z') = \int_{-\infty}^{\infty}\Phi^m(r, r')e^{im(z-z')}\,dm, \tag{C3}$$

where the Φ^m denote the Fourier coefficients, and $\bar{r} = \sqrt{\alpha_n/\alpha_r}|m|r$, one obtains

$$\bar{r}^2\frac{\partial^2\Phi^m}{\partial\bar{r}^2} + \bar{r}\frac{\partial\Phi^m}{\partial\bar{r}} - (\bar{r}^2 + 1)\Phi^m = -\frac{\sqrt{\alpha_r/\alpha_n}}{2\pi|m|}\bar{r}^2\delta(\bar{r} - \bar{r}'). \tag{C4}$$

The solution of this equation that satisfies the boundary condition at $r = 0$ is

$$\Phi^m(\bar{r}, \bar{r}') = \frac{\sqrt{\alpha_r/\alpha_n}}{2\pi|m|}\frac{K_1(\bar{r}_>)I_1(\bar{r}_<)}{K_1(\bar{r}')I_o(\bar{r}') + K_o(\bar{r}')I_1(\bar{r}')}, \tag{C5}$$

where the K_i and I_i are the modified Bessel functions of ith order, and $\bar{r}_>$ and $\bar{r}_<$ denote the larger and smaller of $\bar{r}$ and $\bar{r}'$, respectively. The full solution of (C2) is obtained by performing the integral (C3) over all Fourier coefficients. The condition for ψ at the lower boundary is equivalent to $\partial\Phi/\partial z = 0$ at $z = 0$. It is implemented by adding a mirror charge at $-z'$, yielding

$$\Phi(r, z; r', z') = 4\int_0^{\infty}\Phi^m(r, r')\cos mz'\cos mz\,dm, \tag{C6}$$

where $\Phi^m = \Phi^{-m}$ was used.

The Fourier component of the vertical wind is

$$w^m(r, r') = \frac{1}{r\rho_0}\frac{\partial\psi^m}{\partial r} = \frac{1}{\rho_0}\frac{\partial(r\Phi^m)}{r\partial r}. \tag{C7}$$

Right on the vortex axis ($r = 0$) this gives

$$w^m(0, r') = \frac{1}{2\pi\rho_0}\Theta\left(\sqrt{\frac{\alpha_r}{\alpha_n}}|m|r'\right), \tag{C8}$$

where

$$\Theta(x) = \frac{K_1(x)}{K_1(x)I_o(x) + K_o(x)I_1(x)} \tag{C9}$$

and where $x^{-1}d(xI_1)/dx = I_o(x) = 1$ at $x = 0$ was used. It follows that

$$w(0, z; r', z') = 4\int_0^\infty w^m(0, r')\cos mz'\cos mz\, dm$$

$$= \frac{2}{\pi\rho_0 r'}\sqrt{\frac{\alpha_r}{\alpha_n}}\int_0^\infty \Theta(x)\cos\left(\sqrt{\frac{\alpha_r}{\alpha_n}}\frac{z'}{r'}x\right)\cos\left(\sqrt{\frac{\alpha_r}{\alpha_n}}\frac{z}{r'}x\right)dx. \quad \text{(C10)}$$

Figure 7 shows a numerical evaluation of the integral on the right-hand side for $\alpha_n = 0.1$ day^{-1}, $r' = 500$ km, $z' = 8$ km $\times N_o/f$, $z = 22$ km $\times N_o/f$, and $N_o/f = 120$, that is, for values of the relevant parameters that approximately correspond with the numerical solution shown in Fig. 6b. Apparently, the functional dependence on α_r in the numerical solution is borne out rather well by the Green's function solution. In particular the maximum appears at about the right value of α_r.

Expression (C10) can be used to study the asymptotic behavior of $w(0, z; r', z')$ in α_r. The known asymptotic behavior of K_i and I_i gives

$$\Theta(x) \sim \begin{cases} 1 & \text{for } x \to 0, \\ \left(\dfrac{\pi}{2}x\right)^{1/2} e^{-x} & \text{for } x \to \infty. \end{cases} \quad \text{(C11)}$$

The exponential decay of $\Theta(x)$ at large x ensures that the integral in (C11) is finite. For small values of α_r both cosines in (C10) can be approximated by unity, thus yielding

$$w(0, z; r', z') \sim \frac{2}{\pi\rho_0 r'}\sqrt{\frac{\alpha_r}{\alpha_n}}\int_0^\infty \Theta(x)\, dx$$

$$\sim \text{const.} \times \sqrt{\alpha_r} \quad \text{for } \alpha_r \to 0. \quad \text{(C12)}$$

In the special case of $z = z'$, the leading asymptotic behavior for $\alpha_r \to \infty$ is similar, because $\cos^2\varphi = [1 + \cos(2\varphi)]/2$ and the rapid oscillations of $\cos(2\varphi)$ do not contribute to leading order:

$$w(0, z'; r', z') \sim \frac{1}{\pi\rho_0 r'}\sqrt{\frac{\alpha_r}{\alpha_n}}\int_0^\infty \Theta(x)\, dx$$

$$\sim \text{const.} \times \sqrt{\alpha_r} \quad \text{for } \alpha_r \to \infty \qquad (z = z'). \quad \text{(C13)}$$

On the other hand, for $z \neq z'$ one obtains

$$w(0, z; r', z') \sim \sum_{j=1}^{2} T_j \quad \text{(C14)}$$

with

$$T_j = \frac{1}{\pi\rho_0\tilde{z}_j}\int_0^\infty \Theta\left(\sqrt{\frac{\alpha_n}{\alpha_r}}\frac{r'}{\tilde{z}_j}y\right)\cos y\, dy$$

$$\text{for } \alpha_r \to \infty \qquad (z \neq z'), \quad \text{(C15)}$$

where $\tilde{z}_j = z - z'$ for $j = 1$, $\tilde{z}_j = z + z'$ for $j = 2$, and $y = \sqrt{\alpha_r/\alpha_n}\tilde{z}_j x/r'$. The integral on the right-hand side is evaluated by dividing the interval $[0, \infty)$ into an infinite number of subintervals of length 2π. For large α_r the function Θ can be approximated in each subinterval i by a Taylor series according to

$$\Theta(x) = \Theta(x_{oi}) + (x - x_{oi})\Theta'(x_{oi}) + \frac{(x - x_{oi})^2}{2}\Theta''(x_{oi}) + O(x - x_{oi})^3, \quad \text{(C16)}$$

where $\Theta'(x) = d\Theta/dx$ and x_{oi} denotes the midpoint of subinterval i. The first two terms of the expansion, multiplied by the cosine and integrated over each subinterval, give zero, leaving

$$T_j \sim \frac{1}{\pi\rho_0\tilde{z}_j}\sum_i \frac{1}{2}\frac{\alpha_n r'^2}{\alpha_n\tilde{z}_j^2}4\pi\Theta''(x_{oi})$$

$$\approx \frac{1}{\pi\rho_0\tilde{z}_j}\int_0^\infty \frac{\alpha_n r'^2}{\alpha_n\tilde{z}_j^2}\Theta''\left(\sqrt{\frac{\alpha_r}{\alpha_n}}\frac{r'}{\tilde{z}_j}y\right)dy$$

$$= \frac{r'}{\pi\rho_0\tilde{z}_j^2}\sqrt{\frac{\alpha_n}{\alpha_r}}\int_0^\infty \Theta''(x)\, dx$$

$$= -\frac{r'}{\pi\rho_0\tilde{z}_j^2}\sqrt{\frac{\alpha_n}{\alpha_r}}\Theta'(0) \quad (\text{for } j = 1, 2) \quad \text{(C17)}$$

to leading order in α_r. At the upper limit, $\Theta'(x) \to 0$ as $x \to \infty$ was used. Since $\Theta'(0) = 0$, it follows that

$$w(0, z; r', z') \ll \frac{1}{\sqrt{\alpha_r}} \quad \text{for } \alpha_r \to \infty \qquad (z \neq z'), \quad \text{(C18)}$$

where the $\ll$ refers to the asymptotic behavior in α_r, that is, $\sqrt{\alpha_r}w \to 0$ for $\alpha_r \to \infty$ (cf. Bender and Orszag 1978).

APPENDIX D

Approximate Analytical Theory for the AMC Solution

With $x = r/r_o$, Eq. (46) becomes

$$\overline{T}_a(x) = T_{ao} - \frac{\pi}{2}T_c x^2, \quad \text{(D1)}$$

while the vertical average of (19) yields

$$\overline{T}'_e(x) = \begin{cases} T_{eo}\pi^{-1}(1 + \cos\pi x) & \text{for } x \leq 1, \\ 0 & \text{for } x > 1. \end{cases} \quad \text{(D2)}$$

Requiring continuity of the vertical mean temperature at x_a, that is, $\overline{T}_a(x_a) = \overline{T}_e(x_a)$, gives

$$T_{ao} - \frac{\pi}{2} T_c x_a^2 = \begin{cases} T_{eo}\pi^{-1}(1 + \cos\pi x_a) & \text{for } x_a \le 1, \\ 0 & \text{for } x_a > 1, \end{cases} \tag{D3}$$

and condition (50) becomes

$$\int_0^{x_*} \frac{T_{eo}}{\pi}(1 + \cos\pi x)x\, dx = \int_0^{x_a} (T_{ao} - \frac{\pi}{2} T_c x^2)x\, dx, \tag{D4}$$

where $x_* = \min(x_a, 1)$. By evaluating the integrals in (D4) and using (D3) to eliminate T_{ao} one obtains

$$\frac{8}{\pi^3} x_* \sin\pi x_* + \frac{8}{\pi^4}(\cos\pi x_* - 1) - \frac{4}{\pi^2} x_*^2 \cos\pi x_* = \frac{T_c}{T_{eo}} x_a^4, \tag{D5}$$

which is an algebraic equation for x_a when T_c and T_{eo} are known. Inserting the value of x_a thus calculated into (D3) yields T_{ao}.

The forcing amplitude T_{eo} for which $r_a = r_o$ is obtained by setting $x_a = 1$ in (D5), which gives

$$\frac{T_{eo}}{T_c} = \frac{\pi^2}{4}\left(1 - \frac{4}{\pi^2}\right)^{-1}. \tag{D6}$$

REFERENCES

Becker, E., G. Schmitz, and R. Geprägs, 1997: The feedback of midlatitude waves onto the Hadley cell in a simple general circulation model. *Tellus,* **49A,** 182–199.

Bender, C. M., and S. A. Orszag, 1978: *Advanced Mathematical Methods for Scientists and Engineers.* McGraw-Hill, 593 pp.

Bishop, C. H., and A. J. Thorpe, 1994: Potential vorticity and the electrostatics analogy: Quasi-geostrophic theory. *Quart. J. Roy. Meteor. Soc.,* **120,** 713–731.

Dunkerton, T. J., 1989: Nonlinear Hadley circulation driven by asymmetric differential heating. *J. Atmos. Sci.,* **46,** 956–974.

Eliassen, A., 1952: Slow thermally or frictionally controlled meridional circulation in a circular vortex. *Astrophys. Norv.,* **5** (2), 19–60.

Held, I. M., and A. Y. Hou, 1980: Nonlinear axially symmetric circulations in a nearly inviscid atmosphere. *J. Atmos. Sci.,* **37,** 515–533.

Hou, A. Y., and R. S. Lindzen, 1992: The influence of concentrated heating on the Hadley circulation. *J. Atmos. Sci.,* **49,** 1233–1241.

Hsu, C. J., and R. A. Plumb, 1997: Non-axisymmetric thermally-driven circulations. Preprints, *11th Conf. on Atmospheric and Oceanic Fluid Dynamics,* Tacoma, WA, Amer. Meteor. Soc., 59–61.

Hunt, B. G., 1973: Zonally symmetric global general circulation models with and without the hydrologic cycle. *Tellus,* **25,** 337–354.

Lindzen, R. S., and A. Y. Hou, 1988: Hadley circulations for zonally averaged heating centered off the equator. *J. Atmos. Sci.,* **45,** 2416–2427.

McClatchey, R. A., R. W. Fenn, J. E. A. Selby, F. E. Volz, and J. S. Garin, 1972: Optical properties of the atmosphere (3d ed.). AFCRL-047297, 108 pp. [NTIS AD753075.]

Plumb, R. A., and A. Y. Hou, 1992: The response of a zonally symmetric atmosphere to subtropical thermal forcing: Threshold behavior. *J. Atmos. Sci.,* **49,** 1790–1799.

Raymond, D. J., 1994: Convective processes and tropical atmospheric circulations. *Quart. J. Roy. Meteor. Soc.,* **120,** 1431–1455.

Schneider, E. K., 1977: Axially symmetric steady-state models of the basic state for instability and climate studies. Part II: Nonlinear calculations. *J. Atmos. Sci.,* **34,** 280–296.

——, 1987: A simplified model of the modified Hadley circulation. *J. Atmos. Sci.,* **44,** 3311–3328.

Schubert, W. H., and J. J. Hack, 1983: Transformed Eliassen balanced vortex model. *J. Atmos. Sci.,* **40,** 1571–1583.

Shine, K., 1987: The middle atmosphere in the absence of dynamical heat fluxes. *Quart. J. Roy. Meteor. Soc.,* **113,** 603–633.

Ting, M., 1994: Maintenance of northern summer stationary waves in a GCM. *J. Atmos. Sci.,* **51,** 3286–3308.

Wirth, V., 1995: Diabatic heating in an axisymmetric cut-off cyclone and related stratosphere-troposphere exchange. *Quart. J. Roy. Meteor. Soc.,* **121,** 127–147.

Zhou, X., and L. Chao, 1994: Ozone valley over Tibetan plateau. *Acta Meteor. Sinica,* **8,** 505–506.

Zou, H., 1996: Seasonal variation and trends of TOMS ozone over Tibet. *Geophys. Res. Lett.,* **23,** 1029–1032.